Research Square

Preprints are preliminary reports that have not undergone peer review.
They should not be considered conclusive, used to inform clinical practice,
or referenced by the media as validated information.

Hcfc1a regulates neural precursor proliferation and asxl1 expression in the developing brain.

Victoria L. Castro
The University of Texas at El Paso
Joel F. Reyes
The University of Texas at El Paso
Nayeli Reyes-Nava
The University of Texas at El Paso
David Paz
The University of Texas at El Paso
Anita M Quintana (aquintana8@utep.edu)
The University of Texas at El Paso https://orcid.org/0000-0002-3596-1587

Research article

Keywords: HCFC1, neural precursor cells (NPCs), brain development, asxl1

Posted Date: February 4th, 2020

DOI: https://doi.org/10.21203/rs.2.18231/v2

License: This work is licensed under a Creative Commons Attribution 4.0 International License.
Read Full License

Abstract

Background: Precise regulation of neural precursor cell (NPC) proliferation and differentiation is essential to ensure proper brain development and function. The HCFC1 gene encodes a transcriptional co-factor that regulates cell proliferation, and previous studies suggest that HCFC1 regulates NPC function. However, the molecular mechanism underlying these cellular deficits has not been completely characterized. Methods: Here we created a zebrafish harboring mutations in the hcfc1a gene (the hcfc1a co60/+ allele), one ortholog of HCFC1 and utilized immunohistochemistry and RNA-sequencing technology to understand the function of hcfc1a during neural development. Results: The hcfc1a co60/+ allele results in an increased number of NPCs, neurons, and radial glial cells. These deficits are associated with the abnormal expression of asxl1 , a polycomb transcription factor, which we identified as a downstream effector of hcfc1a using high throughput RNA sequencing technology. Inhibition of asxl1 activity and/or expression in larvae harboring the hcfc1a co60/+ allele completely restored the number of NPCs to normal levels. Conclusion: Collectively, our data demonstrate a novel pathway in which hcfc1a regulates NPCs and neurogenesis.

Background

Neural precursor cells (NPCs) give rise to the differentiated cells of the central nervous system and defects in the number produced, their proliferation, and/or survival can result in a variety of neural developmental disorders. These disorders include intellectual disability (1), cognitive dysfunction (2), behavioral impairment (3), microcephaly (4), epilepsy (5), autism spectrum disorders (6), and cortical malformations (7). Previous studies have demonstrated a complex network of transcription factors that are responsible for modulating NPC function including SOX2 (8), SOX1 (9), NESTIN (10), and PAX transcription factors (11). Recent evidence suggests that the *HCFC1* gene, which encodes a transcriptional cofactor, is essential for stem cell proliferation and metabolism (12,13) in a variety of different tissue types, including neural precursors (14–17). These data strongly suggest that HCFC1 is part of a more global transcriptional program modulating NPC proliferation and differentiation.

HCFC1 regulates a diverse array of target genes and has been shown to bind to the promoters of more than 5000 unique downstream target genes (18). Consequently, the molecular mechanisms by which HCFC1 regulates NPC proliferation and differentiation are complex. Mutations in *HCFC1* cause methylmalonic acidemia and homocysteinemia, cblX type (*cblX*) (309541). *cblX* is an X-linked recessive disorder characterized by defects in cobalamin (vitamin B12) metabolism, nervous system development, neurological impairment, intractable epilepsy, and failure to thrive (19). Functional analysis of *cblX* syndrome has provided a platform whereby the function HCFC1 in discrete organs and tissues can be elucidated. For example, *in vitro* analysis has demonstrated that HCFC1 regulates metabolism indirectly by regulating the expression of the *MMACHC* gene (12,14,15,19). These data are further supported by *in vivo* analysis using transient knockdown in the developing zebrafish (16,20). Additional mouse models exist and have demonstrated a function for HCFC1 in diverse cell populations (21,22), including a subset of NPCs (17). However, although it is clear that HCFC1 is essential for NPC function (17), previous studies

have not yet determined a mechanistic basis for the cellular phenotypes observed. Thus, additional studies examining the function of HCFC1 in NPCs are warranted.

We have created a zebrafish harboring a mutation in the *hcfc1a* gene (*hcfc1a*$^{co60/+}$ *allele) using CRISPR/Cas9. Zebrafish have two orthologs of HCFC1 and in previous studies, we demonstrated that hcfc1b is important for NPC function* (16). The two zebrafish paralogs have been shown to have divergent functions, as the knockdown of *hcfc1b* causes facial dysmorphia, but knockdown of *hcfc1a* does not (20). Therefore, we asked whether germline mutations in the *hcfc1a* gene cause defects in neural development. Our results demonstrate that the *hcfc1a*$^{co60/+}$ *allele* results in increased numbers of proliferating NPCs (Sox2+) and hypomotility. Subsequent RNA sequencing on whole brain homogenates obtained from the *hcfc1a*$^{co60/+}$ *allele* identified increased expression of *asxl1*, which encodes a transcription factor known to modulate the cell cycle (23,24). Furthermore, inhibition of *asxl1* expression in larvae carrying the *hcfc1a*$^{co60/+}$ *allele restored the number of NPCs to normal levels.* Collectively, our study demonstrates a molecular mechanism by which *hcfc1a* regulates NPC proliferation and brain development.

Methods

Experimental Model and Subject Details

The experimental model used in this study is the zebrafish, *Danio rerio*. The *hcfc1a*$^{co60/+}$ allele was produced using CRISPR/Cas9 methodology as described (25). Briefly, a guide RNA (GGTTCATACCAGCCGTTCGT) was designed using publicly available software (ZiFit) (26). Oligonucleotides from the forward and reverse strand were annealed and ligated into the DR274 vector as described (27). Guide template DNA was synthesized using PCR amplification with primers (DR274 FWD: TTTGAGACGGGCGACAGAT and DR274 Rev: TTCTGCTATGGAGGTCAGGT) and RNA was synthesized using the MEGAscript T7 *in vitro* transcription kit. Cas9 was synthesized using the T7 mMessage machine after linearization with PmeI (New England Biolabs) of the Cas9 vector (pMLM3613). A solution (0.2M KCl with phenol red indicator) containing a final concentration of 500ng Cas9 and 70 ng of guide RNA was injected at a volume of 2nL into the single celled embryo and the embryos were grown to adulthood. The *hcfc1a*$^{co60/+}$ *allele was generated from a single founder (F_0), which was outcrossed with 3 independent wildtype (AB) fish to generate 3 families of F1 carriers. Each family consisted of approximately 20 total fish with equal numbers of males and females. To generate subsequent generations, we outcrossed a minimum of 3 F1 individuals with wildtype (Tupfel Long Fin) to obtain a minimum of 3 families of F2 carriers. We subsequently outcrossed F2 carriers (minimum of 3) with wildtype (AB) fish to produce an F3 generation of approximately 3 total families with equal numbers of males and females.* Sanger sequencing confirmed mutation and experiments were initiated in the F3 generation.

The *Tg*(*hsp701*:*HCFC1*) was created using Gateway cloning technology. Briefly, the p5e-*hsp701*, pME-*HCFC1* (created from pcDNA6.1 reported in (20)), p3E-polyA, and the pDestTol2PA were recombined via

LR recombination. The resultant vector was co-injected with transposase mRNA synthesized from the pCS2FA vector as previously described (28). The experiments described herein were performed in the F2 generation, which was produced from a single founder (F_0). The positive F_0 carrier was outcrossed with wildtype (AB) to produce 2 families of F1 individuals and a minimum of 3 carriers of the F1 generation were outcrossed to produce 3 families of F2 carriers that were utilized for the experiments described.

For all experiments, embryos (prior to sexual dimorphism) were obtained by crossing AB wildtype, Tupfel Long Fin wildtype, *Tg*(*hsp701*:*HCFC1*), or *hcfc1a*$^{co60/+}$. Experiments were performed at developmental stages only (0-5DPF). All embryos were maintained in embryo medium at 28° C.

Genotyping

Genotyping of the *hcfc1a*$^{co60/+}$ allele was performed by lysing excised larval tissue or fin clips (adults) in lysis buffer (10mM Tris pH 8.2, 10mM EDTA, 200mM NaCl, 0.5% SDS, and 200ug/ml proteinase K) for 3 hours at 55° C. DNA was isolated according to standard phenol chloroform : ethanol precipitation procedures. Primers pairs were developed that specifically bind to and amplify the mutated allele and did not amplify the wildtype allele. The fragment of interest was amplified by standard PCR at an annealing temperature of 64° (FWD: CCAGTTCGCCTTTTTGTTGT and REV: ACGGGTGGTATGAACCACTGGC). Positive amplification indicates positive carriers of the allele (Figure 1). Genotyping of the *Tg*(*hsp701*:*HCFC1*) allele was performed with the following primers: forward primer (TGAAACAATTGCACCATAAATTG) present in the *hsp701* promoter and reverse primer in the *HCFC1* open reading frame (CGTCACACACGAAGCCATAG). Amplification indicates the genotype of interest.

Immunohistochemistry

Embryos/larvae were fixed in 4% paraformaldehyde (Electron Microscopy Sciences) for 1 hour at room temperature (RT). For each time point, a small piece of caudal tissue was excised for genotyping and the remaining rostral tissue was embedded in 1.5% agarose (Fisher) produced in 5% sucrose (Fisher) and embryo medium. Embedded blocks were incubated overnight in 30% sucrose (Fisher) and then snap frozen with dry ice and cryosectioned (12-20uM). Sections were washed twice in 1X phosphate buffered saline (PBS) pH 7.4 at RT for 30 minutes each and blocked for 1 hour in blocking buffer (2mg/ml bovine serum albumin (Fisher), 2% goat serum (Fisher) diluted in 1X PBS). Primary antibody (1:200 anti-Sox2 (Abcam) or 1:500 anti-HuC/D (Fisher) was incubated overnight at 4◦C and then washed twice in 1X PBS for 30 minutes each at RT. Alexa fluor antibodies (Fisher) were diluted 1:200 and incubated on each slide for 1 hour at RT. All slides were cover slipped using Vectashield (Vector Laboratories) and imaged on a Zeiss LSM 700 at 20X-63X magnification. For cell proliferation, larvae were pulsed in 20mM EdU (Fisher) diluted in 10% dimethyl sulfoxide (DMSO) (Fisher) for 30 minutes at RT prior to fixation. EdU was detected using the EdU Click-It technology (Fisher) according to manufacturer protocol.

Cell Quantification

For cell quantification, sections were first divided into forebrain, midbrain, and hindbrain regions using two zebrafish brain atlases 1) Atlas of Zebrafish Development (29) and 2) Atlas of Early Zebrafish Brain Development (30). To specify brain regions, major hallmark sub-divisions of each brain section were separated based on age of larvae and the published sections and demarcations present in (30). For example, sections of the developing brain are organized by letters: A-F indicate forebrain sections, G-L are midbrain, and M-R are hindbrain according to the zebrafish brain atlas. After standardization of the brain region by atlas, cells from each section (12-20uM) were counted using the ImageJ cell counter. The ImageJ cell counter allows for the manual counting of cells by marking each cell with a colored square and adds the tallied cell to the quantification sheet. The cell counter allows for the tally of 4 independent groups separately with a different color square. Cells were easily visible across all replicates. Only biological replicates with high tissue integrity were quantified. For comparison of representative images, equivalent sections are shown to ensure that minor changes in tissue geometry do not affect the overall conclusion. These sections are standardized from the zebrafish brain atlas. For bar graphs, the average number of cells across each brain region were utilized for quantification using approximately, 10-20 equivalent sections/brain region/fish were quantified. The number of animals per group is described in each figure legend. To determine the relative increase/decrease in total cell number, the number of total cells/section was divided by the average number of cells present in wildtype siblings for each brain region analyzed and multiplied by 100. All statistical analysis was performed using total numbers of cells/section/brain region. All immunohistochemistry was validated with quantitative real time PCR (QPCR) of each gene analyzed.

QPCR and in situ hybridization

Whole mount *in situ* hybridization (ISH) was performed as described by Thisse and Thisse (31). Briefly, embryos were harvested and dechorionated at the indicated time point and fixed in 4% paraformaldehyde (PFA) (Electron Microscopy Sciences) for 1 hour at room temperature (RT). Embryos were permeabilized with proteinase K (10ug/ml) for the time indicated by Thisse and Thisse (32). Permeabilized embryos were prehybridized in hybridization buffer (HB) (50% deionized formamide (Fisher), 5X SSC (Fisher), 0.1% Tween 20 (Fisher), 50mg ml^{-1} heparin (Sigma, St. Louis), 500mg ml^{-1} of RNase-free tRNA (Sigma), 1M citric acid (Fisher) (460ml for 50ml of HB)) for 2-4 hours and then incubated overnight in fresh HB with probe (50-100ng) at 70°C. Samples were washed, blocked in 2% sheep serum, and incubated with anti-DIG Fab fragments (1:10,000) (Sigma) overnight at 4°C. Samples were developed with BM purple AP substrate (Sigma) and images were collected with a Zeiss Discovery Stereo Microscope fitted with Zen Software. *The asxl1* cDNA probe sequence was amplified using the following primers: FWD: CATCAACACACGGACCTTTG and REV: CAGTGAGTGGGGTGGAAGTT, purified using a DNA purification kit (Fisher), then ligated into the pGEM-T easy vector using the pGEM T-easy Plasmid Ligation Kit (Promega).

For QPCR, RNA was isolated from embryos at the indicated time point using Trizol (Fisher) according to manufacturer's protocol. Reverse transcription was performed using Verso cDNA synthesis (Fisher) and total RNA was normalized across all samples. PCR was performed in technical triplicates for each sample using an Applied Biosystem's StepOne Plus machine with Applied Biosystem's software. Sybr

green (Fisher) based primer pairs for each gene analyzed are as follows: *mmachc* fwd: GCTTCGAGGTTTACCCCTTC, *mmachc* rev: AGGCCAGGGTAGGGTCCTG, *hcfc1a* fwd: ACAGGGCCTAACACAGGTTG, *hcfc1a* rev: TCCTGTGACTGTGCCAAGAG, *asxl1* fwd: CCAGAGCTGGAAAGAACGTC, *asxl1* rev: ACATCTCCAGCTTCGCTCAT, *rpl13a* fwd: TCCCAGCTGCTCTCAAGATT, *rpl13a* rev: TTCTTGGAATAGCGCAGCTT, *sox2* fwd: AACTCCTCGGGAAACAACCA, *sox2* rev: ATCCGGGTGTTCCTTCATGT, *elavl3* fwd: TAACGGCCCTGTCATTAGCA, *elavl3* rev: CGTGTTGATAGCCTTGTCGG, *gfap* fwd: GGCCAACTCTAACATGCAGG, *gfap* rev: ATTCCAGGTCACAGGTCAGG, *olig2* fwd: TTCTGTAGGCCACACACCAG, and *olig2* rev: TTAACTCCGGTGGAGAATCG. Analysis was performed using 2^{DDct}.

For RNA sequencing analysis, total RNA was isolated from brain homogenates (N=12/group from 3 biological replicates), analyzed for RNA integrity, and sequenced at The University of Texas El Paso Border Biomedical Research Center Genomics Core Facility. RNA sequencing was performed in biological triplicate. RNA integrity was assessed with a TapeStation 2200 and the library was prepared with a TruSeq stranded mRNA library preparation kit. Sequencing was performed on a NextSeq500 (Illumina) using a high output kit V2 (150 cycles). For analysis, the sequences were quality trimmed using Trimmomatic (33) and aligned to the Danio *rerio* genome (build GRCz11) obtained from Ensembl v95 using Tophat2 (34). Cufflinks (35) was used to determine the differential expression patterns between mutant and wildtype samples.

Tg(*hsp701*:*HCFC1*) analysis and rescue experiments.

F2 carriers of the *Tg*(*hsp701*:HCFC1) were incrossed and grown at 28° for 24 hours and then split into two groups, non-heat shock and heat shock. Heat shock was performed for 30 minutes at 38° and then allowed to acclimate at room temperature for 20 minutes. Heat shock was initiated at 24 hours post fertilization (HPF) and performed every 8 hours until 5 days post fertilization (DPF). For LY294002 (Selleck Chemicals) rescue, the drug was dissolved in 100% Dimethyl-Sulfoxide (DMSO) (Fisher) and embryos were treated at 24 HPF with a 12uM concentration for a period of 24 hours. Media was removed and embryos were dechorionated and fixed for immunohistochemistry.

For morpholino rescue, 2 nL of a 0.1 mM solution of *asxl1* targeting translation inhibiting morpholinos (GTTTGTCCTTCATTTCCTCAGTGTT) or random control morpholinos (Gene-Tools) were injected into offspring of the *hcfc1a*$^{co60/+}$ allele. Injected embryos were fixed at 2 DPF and simultaneously stained for the number of Sox2+ and/or EdU+ positive cells. Cells were counted as described above.

Larval Behavioral Assay

Embryos were obtained from an outcross of the *hcfc1a*$^{co60/+}$ allele and raised to 5 DPF. Behavioral quantification was performed using the Zebrabox (ViewPoint Behavior Technology). Larvae were individually tracked for swim speed and total distance swam in a 96 well plate. The behavioral protocol

was a total of 15 minutes divided into 5 minute intervals of dark/light/dark conditions. All larvae were acclimated to the dish and housing conditions for 1 hour prior to analysis. Settings for the program include a threshold of 16 and integration period of 300 seconds. Data was measured as total distance traveled (mm) and total swim speed (mm/sec) (Swim Speed= {Total distance traveled in large and small movements) (Smldist+Lardist)}/{Total duration spent by the animal in small and large movements (smldur+lardur)}. Statistical significance was determined according to a T-test. All experiments were performed in biological triplicate.

Quantification and Statistical Analysis

For all assays, statistical significance was calculated using a Student's T-test to compare the means of two groups. All assays were performed in biological duplicate and triplicate and all QPCR was performed in technical triplicate. For each assay, the total number of animals (N) is indicated in the figure legend. Number of animals was determined based on power analysis conducted from preliminary studies. For all graphs, statistical significance between groups and the P-value is demonstrated in the figure legends. For cell quantification, the number of Sox2+ or EdU+ cells were counted per section and normalized according to the Methods Section above. All sections were sub-divided based on landmarks in the Atlas of Early Zebrafish Brain Development, 2nd Edition and then separated into specific brain regions (forebrain, midbrain, and hindbrain). All graphs represent error bars as standard error of the mean (SEM).

Results

Production of the *hcfc1a$^{co60/+}$ allele.*

Previous studies suggest that HCFC1 regulates NPC function *in vitro* and in mouse models (14–17). *HCFC1* is highly conserved across species (19) and zebrafish have been used in previous reports as a model system to understand the mechanisms by which mutations in *HCFC1* cause disease (16,20). Therefore, we developed a zebrafish harboring a germline mutation in the *hcfc1a* gene using CRISPR/Cas9 technology. We developed a specific guide RNA (sgRNA) that targets exon 4 of the *hcfc1a* gene (Figure 1A). The sgRNA was injected at the single cell stage and resulted in the net insertion of 13 nucleotides (Figure 1A). The introduction of these nucleotides is predicted to introduce a premature stop codon and encode a peptide of 94 amino acids in length (Supplemental Figure 1). Full length Hcfc1a is 1778 amino acids in length. Genotyping of the *hcfc1a$^{co60/+}$* allele was developed according to the Materials and methods section, using a reverse primers unique to the mutant allele in the amplification strategy (Figure 1A). Positive amplification was indicative of positive carriers (Figure 1B), as the primers did not bind to or amplify the wildtype allele. Initial crosses between heterozygous carriers of the *hcfc1a$^{co60/+}$ failed to generate homozygous progeny and* did not obey Mendelian inheritance patterns. These results indicate that Hcfc1a is required for early development, which is consistent with previously published studies (21,22), however the mechanism for embryonic lethality of the homozygous allele was not explored further here. However, since knockdown of *hcfc1a* is not homozygous lethal (20), we surmised that heterozygous carriers of the *hcfc1a$^{co60/+}$* allele would have defects in overall *hcfc1a*

expression and potential defects in brain development. Therefore, we measured the expression of *hcfc1a* in carriers of the *hcfc1a*$^{co60/+}$ allele and their wildtype siblings using QPCR. We designed primers to detect *hcfc1a* expression downstream of Exon 4 that span exons 15 and 17 so as to ensure that such primers were capable of detecting changes in total mRNA expression and not deficiencies in Exon 4 only. As shown in Figure 1C, at 2 DPF carriers of the *hcfc1a*$^{co60/+}$ allele had a 50% decrease in total *hcfc1a* mRNA ($P<0.05$).

Hcfc1a regulates NPC number *in vivo*.

Several studies suggest that mutation or disruption of *Hcfc1* (mouse) mRNA disrupts NPC function. Moreover, we have previously published that *hcfc1a* is expressed in the developing brain across the forebrain, midbrain, and hindbrain (20). Therefore, we asked whether the decrease in *hcfc1a* mRNA expression in carriers of the *hcfc1a*$^{co60/+}$ resulted in abnormal NPC development *in vivo.* To test this, we first measured the expression of *sox2* and *pax6* using QPCR at 5 DPF. We used *sox2* and *pax6* as a readouts for NPCs because they are co-localized and established markers of NPCs in the field (36–38). At 5 DPF, the expression of both *sox2* and *pax6* were up-regulated in *hcfc1a*$^{co60/+}$ larvae relative to their wildtype siblings (Figure 2A). We next compared the total number of Sox2+ cells in *hcfc1a*$^{co60/+}$ larvae and their wildtype siblings over the course of development at 1, 2, and 5 DPF. Increased NPCs were not observed until 2 DPF (Figure 2C) and were sustained until 5 DPF (Figure 2D). *hcfc1a*$^{co60/+}$ larvae had increased numbers of NPCs in the forebrain, midbrain, and hindbrain regions, with NPCs highly enriched in the ventricular region of the developing brain (Figure 2E-H and E'-F', arrowheads indicate cells). There was approximately 25-30% more Sox2^{+} cells per brain region based upon our quantification (Figure 2).

The hcfc1a$^{co60/+}$ *allele disrupts cell proliferation.*

Based upon previously published data (17), we hypothesized that the excess NPCs produced undergo cell death. To measure cell death, we performed immunohistochemistry with anti-active caspase 3 antibodies and anti-Sox2 antibodies. As shown in Figure 3A and 3A', we detected approximately 1-2 Caspase+ Sox2+ cells in sibling controls, however larvae harboring the *hcfc1a*$^{co60/+}$ *allele* had on average approximately 5 co-localized cells per/section. As we detected very few total caspase+ NPCs, we next quantified the total number of NPCs in each group to determine the total number of NPCs surviving. As shown in Figure 3B, while the *hcfc1a*$^{co60/+}$ *allele led to an increase in the number of caspase positive NPCs (red bars), the vast majority of NPCs in both wildtype and hcfc1a*$^{co60/+}$ *larvae were not caspase positive (gray bars), indicating that a significant fraction of NPCs survive. Because of this survival, we next analyzed cell proliferation in hcfc1a*$^{co60/+}$ larvae and their wildtype siblings using 5-ethynyl-2'-deoxyuridine (EdU) and EdU click-it technology. The *hcfc1a*$^{co60/+}$ allele resulted in a statistically significant increase in the number of EdU positive cells in both the midbrain and hindbrain regions (Figure 3C-D & 3C'-D' and quantified in Figure 3E). We observed an increase in the number of EdU positive cells in the forebrain, although the increase in the forebrain was not significant across multiple biological replicates ($P=0.06$). Collectively,

these data suggest the *hcfc1a*$^{co60/+}$ allele results in an increase in NPC proliferation, whereby a sub-population of these NPCs undergo cell death, while the majority of those NPCs produced, survive.

The *hcfc1a*$^{co60/+}$ allele is associated with abnormal expression of pro-neural and pro-glial genes.

The *hcfc1a*$^{co60/+}$ allele is associated with increased proliferation and an increased number of NPCs. Importantly, the majority of these cells did not undergo cell death and therefore, we asked if the expression of genes associated with differentiation was abnormal. We measured the expression of 2 established markers of neurons and radial glial cells, *elavl3* and *gfap* by immunohistochemistry. As shown in the Figure 4A'&B', Gfap and Elavl3 expression were increased in *hcfc1a*$^{co60/+}$ larvae at 5 DPF. Next, we quantified the level of expression of each marker and one additional marker of differentiation (*olig2*) using QPCR at 5DPF. QPCR demonstrated an increase in the level of mRNA expression of each marker (Figure 4C) in *hcfc1a*$^{co60/+}$ larvae relative to their wildtype siblings ($P<0.05$).

Overexpression of HCFC1 reduces the number of NPCs and decreases neural and glial gene expression.

Our data demonstrates that haploinsufficiency of *hcfc1a* disrupts NPC function. Previous studies have shown that over-expression of Hcfc1 (mouse) *in vitro* has the opposite effect (15). We tested this possibility by creating a transgenic zebrafish expressing human HCFC1 under the control of the heat shock promoter for the *hsp701* gene. The efficacy of the *hsp701* promoter in zebrafish has been widely established in previous studies (28,39–43). We activated expression of HCFC1 by performing a heat shock as described in the methods section for a period of 5 days. We first measured the mRNA expression of *sox2*, *elavl3* (HuC/D), *gfap*, and *olig2* by QPCR. Activation by heat shock of the *Tg*(*hsp701*:HCFC1) allele resulted in decreased expression of all markers analyzed (Figure 5A; $P<0.05$). We next analyzed the number of Sox2+ cells in the presence and absence of heat shock. Activation of the *Tg*(*hsp701*:HCFC1) was associated with a decreased number of NPCs across the forebrain ($P=4.88568E-05$), midbrain ($P=0.004359$), and hindbrain ($P=0.0776$) (Figure 5B, 5C-C').

Asxl1 is overexpressed in animals with the *hcfc1a*$^{co60/+}$ allele.

HCFC1 is known to regulate metabolism and craniofacial development via the modulation of *MMACHC* expression (14,19,20). Therefore, we hypothesized the neural phenotypes associated with mutations in *hcfc1a* were the direct consequence of defects in *mmachc* expression. We measured the expression of *mmachc* in *hcfc1a* mutants and their wildtype siblings in whole brain homogenates. As shown in Figure 6A, QPCR analysis demonstrated that *mmachc* expression was unchanged by the *hcfc1a*$^{co60/+}$ *allele.* Based upon these data, we hypothesized that mutation of *hcfc1a* does not regulate brain development by modulating *mmachc* expression. To better understand the mechanisms downstream of *hcfc1a*, we performed RNA-sequencing at 2 DPF using whole brain homogenates from wildtype and *hcfc1a*$^{co60/+}$ *larvae (Table 1)*. Using literature analysis, we identified the *asxl1* gene as one a possible downstream effector of Hcfc1a in the developing brain. *asxl1* encodes a transcriptional regulator that is essential for proper cell proliferation and whose deletion causes cellular senescence (24,44). More importantly,

mutations in *ASXL1* have been associated with Boring Opitz Syndrome (605039), which has been characterized by profound intellectual disability (45). According to *in situ* hybridization, *asxl1* expression was restricted to the developing zebrafish brain (Figure 6B&B') and QPCR analysis of brain homogenates validated a 14-fold increase of *asxl1* expression at 2 DPF in *hcfc1a*$^{co60/+}$ *larvae* relative to wildtype siblings (Figure 6C).

Inhibition of *asxl1* restores the NPC phenotype in *hcfc1a*$^{co60/+}$ *larvae*.

Deletion of *Asxl1* in mouse embryonic fibroblasts (MEFs) causes growth retardation because Asxl1 regulates the cell cycle via AKT-E2F (24). Based upon these data, we hypothesized that over-expression of *asxl1* in *hcfc1a*$^{co60/+}$ *larvae* promotes proliferation of NPCs. To test this hypothesis, we designed a translational blocking morpholino to inhibit *asxl1* expression in *hcfc1a*$^{co60/+}$ *larvae*. We determined the concentration for injection empirically and selected the highest concentration that promoted >70% survival of injected embryos. We injected *asxl1* morpholinos or random control morpholinos into *hcfc1a*$^{co60/+}$ *larvae* and their wildtype siblings at the single cell stage and we analyzed the number of EdU positive cells at 2 DPF. As shown in Figure 6D, the injection of random control morpholinos into *hcfc1a* mutants and their wildtype siblings had no detrimental effects and recapitulated the NPC phenotype previously observed (i.e. increased NPCs, Figure 2). However, the injection of *asxl1* morpholinos completely restored the number of NPCs to wildtype levels in all brain regions (Figure 6D, red bars).

Morpholinos can display off-target effects (46) and therefore we sought an alternative route of *asxl1* inhibition in *hcfc1a*$^{co60/+}$ *larvae. Youn and colleagues have demonstrated that ASXL1 (mouse) promotes cell proliferation by binding to AKT kinase and promoting AKT phosphorylation* (24) (Figure 7A). However, this function can be inhibited by decreasing the activity of PI3K/AKT. Therefore, we treated *hcfc1a*$^{co60/+}$ *larvae and their wildtype siblings with* LY294002, as described in (24). *hcfc1a*$^{co60/+}$ *embryos were* treated at 24HPF with 12uM LY294002 or vehicle control (DMSO). Vehicle treatment of wildtype and *hcfc1a*$^{co60/+}$ *larvae* recapitulated the NPC phenotype present in *hcfc1a*$^{co60/+}$ *larvae (Figure 7B-B",7C-C", and 7D-D"), which was consistent* across all brain regions as both the number of Sox2+ cells (Figure 7E) and the number of EdU+ cells (Figure 7F) were increased in *hcfc1a*$^{co60/+}$ *larvae*. In contrast, treatment with LY294002 reduced the number of cycling cells (EdU+) and the number of NPCs (Sox2+) in *hcfc1a*$^{co60/+}$ *larvae*, consistent with our hypothesis (Figure 7E&F, red bars). To complement these data, we next performed mRNA expression analysis of *sox2*, *asxl1*, and cyclin E (*ccne1*) in treated and untreated *hcfc1a*$^{co60/+}$ *larvae at 5 DPF.* As shown in Figure 7G, treatment with LY294002 resulted in decreased expression of *sox2* and *asxl1*, which was correlated with decreased cyclin E expression ($P<0.05$).

Defects in neural development are associated with larval hypomotility.

The functional consequences of the defects in brain development in the *hcfc1a*$^{co60/+}$ *allele are not completely understood. However, mutation of HCFC1 in patients with cblX syndrome is associated with movement disorders* (19). Therefore, we performed larval behavioral assays to determine if the defects in

brain development present in larvae with the *hcfc1a$^{co60/+}$ allele were associated with abnormal swim patterns. To test this, we monitored swim behavior of 5 DPF larvae using Zebrabox technology. Upon light stimulus* carriers of the
hcfc1a$^{co60/+}$ allele exhibited reduced overall distance swam, but overall speed was not affected (Figure 8A&B). These behavioral deficits are consistent with a hypomotility phenotype (47). Importantly, *hcfc1a$^{co60/+}$ responded normally to dark-light-dark transitions (Figure 8C) as has been previously demonstrated* (48).

Discussion

Here we demonstrate that the *hcfc1a$^{co60/+}$ allele* results in an increase in the number of NPCs during early brain development. This increase in NPC number is a direct consequence of over proliferation of NPCs. Mutations in *HCFC1* cause *cblX* syndrome, a multiple congenital anomaly syndrome, associated with cobalamin deficiencies and significant neurological deficits, among other phenotypes (15,19). *HCFC1* encodes for a transcriptional co-activator that regulates genes important for metabolism and proliferation (12). It is suggested that HCFC1 binds to and regulates the expression of >5000 different genes (18), with various different interacting partners including THAP11 (13) and ZNF143 (49), where mutation of either can cause a *cblX* like disorder (16,50).

Previous reports suggest that HCFC1 regulates NPC function (14–17). *In vitro*, decreased *Hcfc1* (mouse) expression increases the number of NPCs and reduces the expression of markers associated with differentiation (14). These data are consistent with the known function of *Hcfc1* in cell proliferation (51–53). Mutation of *Hcfc1* (mouse) is embryonically lethal (21) and consequently, the *in vivo* function of HCFC1 has been difficult to characterize. Our results are consistent with this observation as we did not detect homozygous mutant larvae. We sequenced larvae from an incross of *hcfc1a$^{co60/+}$ larvae* at 2, 4, and 8 HPF and even at the earliest time point we detected only heterozygous carriers. We did not explore this mechanism further, however in previous studies the murine Hcfc1 mutant allele was subject to compensatory mechanisms and only the paternally inherited allele was viable (21). Zebrafish do not have sex chromosomes, but future studies are warranted that characterize the inheritance of the *hcfc1a$^{co60/+}$ allele*.

Recently a cell-type specific mutant allele was created in which *Hcfc1* (mouse) was deleted from a sub-population of neural precursors (NKX2.1+). This cell type specific deletion of *Hcfc1* (mouse) induces cell death and defects in differentiation without affecting proliferation. The discrepancy between these results could be explained by many factors including the propagation of neurospheres *in vitro* and the inability to decipher how the developing microenvironment affects normal physiology. However, some studies have helped to shed light on the latter explanation because the *in vivo* knockdown of *hcfc1b*, one of the zebrafish orthologs of *HCFC1*, resulted in increased NPC proliferation (16). Thus, the function of HCFC1 is complex, with several unknown cell-type specific functions that can be affected by the surrounding microenvironment of the developing brain.

Here we developed a zebrafish harboring a germline mutation in the *hcfc1a* gene. We analyzed the effects of this mutation on NPC function. Consistent with the literature (14–16), our allele resulted in an increase in the number of Sox2+ cells and increased cellular proliferation without significant deficits in cell survival. Increased cell proliferation was observed across different brain regions. Strikingly, the increase in NPCs was not associated with increased apoptosis of NPCs, but instead with increased expression of markers associated with neurons and glia. The effects of this increased expression are yet to be elucidated, however studies that provide information on brain volume and the ratio of gray and white matter in the central nervous system are warranted given that the increases in neurons and glia we observed are unique from the differentiation defects observed in previous studies (14,17). However, we suspect the difference in phenotype is associated with the type of mutation introduced, the brain microenvironment, the cell population analyzed, and the region of the brain of interest. For example, Minocha and Herr (17) deleted exons 2 and 3 of *Hcfc1* using a Cre-Lox system with a cell type specific promoter. The resulting approach introduces the formation of a truncated protein, whereas, our system results in decreased overall expression (Figure 1) more consistent with previous *in vitro* assays and haploinsufficiency. However our haploinsufficient allele advances the field because unlike the previous *in vitro* assays (14,15), our allele accounts for the broad expression of Hcfc1 which was recently documented by Minocha and colleagues (17).

HCFC1 regulates a myriad of downstream target genes (12,18) and therefore, the mechanisms by which HCFC1 regulates NPC function are not clear. The majority of the literature focuses primarily on the function of HCFC1 at the *MMACHC* promoter in the human syndrome, *cblX*. *cblX* disorder is the result of mutations in the HCFC1 gene and these mutations disrupt protein function causing a decrease the expression of *MMACHC* and a metabolic disorder (14,19). Interestingly, mutations in *MMACHC* cause *cblC* disorder, which has many overlapping phenotypes with *cblX* including neurodevelopmental defects (54). These data led us to hypothesize that HCFC1 regulates NPC function by modulating MMACHC expression. However, the *hcfc1a*$^{co60/+}$ *allele* did not disrupt *mmachc* expression, however whether our allele causes other metabolic deficits is not known and was not explored further here. For example, mutation of the human HCFC1 gene has been associated with nonketotic hyperglycinemia (55). Collectively the data presented here suggests that the *hcfc1a*$^{co60/+}$ *allele* disrupts NPC function by a novel molecular mechanism. In addition, these data suggest some divergent function between *hcfc1a* and *hcfc1b*, as the latter has been shown to regulate *mmachc* expression and craniofacial development (20).

Our results strongly suggest an *mmachc* independent mechanism underlying the neural developmental phenotypes associated with the *hcfc1a*$^{co60/+}$ *allele*, but we cannot completely rule out that *hcfc1b* regulates brain development via *mmachc* expression or that other factors including cobalamin, homocysteine, or methylmalonic acid function aberrantly as a consequence of mutations in *hcfc1a*. However, RNA-sequencing of brain homogenates provided us a list of potential downstream candidate effectors of *hcfc1a*. Of those candidates, the *asxl1* gene was afforded high priority because of its known role regulating cellular proliferation (24,44,56) and for its documented function in mouse embryonic stem cells and neural differentiation (23). Interestingly, the *hcfc1a*$^{co60/+}$ *allele* causes a 14-fold induction of

asxl1 expression. In mouse embryonic fibroblasts, the deletion of *Asxl1* causes cellular senescence. We observed increased cellular proliferation and therefore, postulated that an increased level of Asxl1 protein was promoting NPC proliferation in *hcfc1a* mutant larvae. Consistent with the known function of *asxl1* and our hypothesis, knockdown of *asxl1* in *hcfc1a* mutant larvae restored the defects in cellular proliferation, resulting in normal numbers of Sox2+ cells.

Interestingly, *ASXL1* has been shown to regulate cell proliferation in other cell types (56,57) and this activity has been associated with activation of AKT. Based upon these data, we attempted to restore the phenotypes present in the *hcfc1a*$^{co60/+}$ allele by inhibiting ASXL1 activity downstream of PI3K (24). Consistent with this role, the inhibition of ASXL1 activity using pharmacological inhibition completely restored the NPC deficits present in *hcfc1a* mutants. Thus, our data suggest a mechanism whereby *hcfc1a* regulates the expression of Asxl1, and the cell cycle during early brain development. However, whether *hcfc1a* regulates *asxl1* by directly binding to the *asxl1* promoter is still not known, but interestingly ASXL1 and HCFC1 interact with one another in myeloid cells to regulate proliferation and differentiation (58). Thus, these two proteins may regulate the activity of one another at multiple levels.

We observed changes in the expression of various markers of neurons and glia. However, the physiological consequences of these changes are currently not known as a viable mouse model has not been developed. Zebrafish have emerged as a model for neurodevelopmental disorders (59) and behavioral assays for seizure (60) and motor deficits (61) have been described. Therefore, we characterized the locomotion of *hcfc1a* mutants in response to light stimulus (62). Our results using Zebrabox technology demonstrated reduced motility as indicated by distance travelled without defects in overall speed. Importantly, the decreased motility with light stimulus was not due to an overall defective response to light, as our analysis demonstrated that carriers of the *hcfc1a*$^{co60/+}$ allele responded to light as indicated by the “V” like pattern in dark-light-dark conditions (63). Decreased distance travelled has been previously defined as hypolocomotion and is associated with motor incoordination (64). Hypolocomotion has been demonstrated in zebrafish models of ALS (61,65) and fetal akinesia (66), two disorders characterized by motor deficits. Interestingly, the hypolocomotion we observed was correlated with increased NPCs and defects in the expression of various markers associated with differentiation. We did not observe short convulsions or whirlpool like behaviors in mutant larvae, which would have been indicative of a seizure phenotype and it is likely that the protocol we used to detect behavior does not stimulate seizure like phenotypes. Future studies that use multiple stimuli, including low dose convulsants will likely shed light on the epileptic phenotypes associated with mutations in *hcfc1a*.

Conclusions

Our study focuses on the function of *hcfc1a*, one ortholog of *HCFC1*, during brain development. Specifically, we focus on the function of *hcfc1a* in modulating NPC number and proliferation. We demonstrate that HCFC1 is essential for the proliferation of NPCs. Importantly, we connect these cellular deficits to a molecular mechanism whereby *hcfc1a* indirectly regulates *asxl1* to control cellular

proliferation. Thus, we propose that our system has the potential to inform about the transcriptional program regulating NPC function.

Abbreviations

NPC: Neural Precursor

cblX: methylmalonic acidemia and homocysteinemia, cblX type

F_0: Founder

DPF: days post fertilization

HPF: hours post fertilization

RT: room temperature

DMSO: dimethylsulfoxide

QPCR: quantitative real time PCR

ISH: whole mount in situ hybridization

SEM: standard error of the mean

EdU: 5-ethynyl-2’-deoxyuridine

mM: millimolar

uM: micromolar

PFA: paraformaldehyde

SSC: saline sodium citrate

DIG: digoxigenin

AP: Alkaline phosphate

CRISPR/Cas9: Clustered Regularly Interspaced short palindromic repeats/Cas9 nuclease

ng: nanograms

nL: nanoliters

EDTA: ethylenediaminetetraacetic acid

NaCl: sodium chloride

SDS: sodium dodecyl sulfate

ug: microgram

PCR: polymerase chain reaction

uM: micromolar

HB: Hybridization buffer

MEF: mouse embryonic fibroblasts

Declarations

Ethics Approval and Consent to Participate

All experiments were performed according to protocol 811689-5 approved by The University of Texas El Paso Institutional Animal Care and Use Committee (IACUC).

Consent to Publish

Not applicable

Availability of Data and Materials

The RNA-sequencing data sets generated during this study have been deposited into the GEO database with accession number GSE132864 and a summary is included within the article. All files are also available from the corresponding author upon request.

Competing Interests

Authors report no competing financial interests.

Funding

These studies were supported by grants from the National Institutes of Health (National Institute on Minority Health and Health Disparities-2G12MD007592 to The University of Texas El Paso, National Institutes of General Medical Sciences RL5GM118969, TL4GM118971, R25GM069621-11, UL1GM118970 to The University of Texas El Paso, and National Institute of Neurological Disorders and Stroke 1K01NS099153-01A1 to Anita M. Quintana. This study was designed, performed, and analyzed by the authors. The funding sources provided financial support for the experiments described.

Author Contributions

AMQ synthesized the hypothesis, wrote the manuscript, analyzed data, performed statistical analysis, genotyped, performed QPCR maintained zebrafish lines. VLC cryosectioned, imaged, counted cells, performed immunohistochemistry, performed injections, drug treatments, RNA analysis and QPCR, and aided in the study design. JFR performed cryosectioning, immunohistochemistry, genotyping, and cell counts. AMQ produced the germline mutant and transgenic heat shock animal. NRN performed cell counts, imaging, and genotyping. DP performed genotyping. All authors read and approved the manuscript before submission.

Acknowledgements

Authors thank and acknowledge the help and support of Valerie Caro, Jose Hernandez, and Tamim Shaikh, and Bruce Appel.

References

1. Trazzi S, Mitrugno VM, Valli E, Fuchs C, Rizzi S, Guidi S, et al. APP-dependent up-regulation of Ptch1 underlies proliferation impairment of neural precursors in Down syndrome. Hum Mol Genet. 2011 Apr 15;20(8):1560–73.
2. Wang J, Weaver ICG, Gauthier-Fisher A, Wang H, He L, Yeomans J, et al. CBP histone acetyltransferase activity regulates embryonic neural differentiation in the normal and Rubinstein-Taybi syndrome brain. Dev Cell. 2010 Jan 19;18(1):114–25.
3. Dugani CB, Paquin A, Kaplan DR, Miller FD. Coffin-Lowry syndrome: a role for RSK2 in mammalian neurogenesis. Dev Biol. 2010 Nov 15;347(2):348–59.
4. Paronett EM, Meechan DW, Karpinski BA, LaMantia A-S, Maynard TM. Ranbp1, Deleted in DiGeorge/22q11.2 Deletion Syndrome, is a Microcephaly Gene That Selectively Disrupts Layer 2/3 Cortical Projection Neuron Generation. Cereb Cortex. 2015 Oct;25(10):3977–93.
5. Roy A, Skibo J, Kalume F, Ni J, Rankin S, Lu Y, et al. Mouse models of human PIK3CA-related brain overgrowth have acutely treatable epilepsy. Elife. 2015;4.
6. Sugathan A, Biagioli M, Golzio C, Erdin S, Blumenthal I, Manavalan P, et al. CHD8 regulates neurodevelopmental pathways associated with autism spectrum disorder in neural progenitors. Proc Natl Acad Sci USA. 2014 Oct 21;111(42):E4468-4477.
7. Paquin A, Hordo C, Kaplan DR, Miller FD. Costello syndrome H-Ras alleles regulate cortical development. Dev Biol. 2009 Jun 15;330(2):440–51.
8. Cimadamore F, Amador-Arjona A, Chen C, Huang C-T, Terskikh AV. SOX2-LIN28/let-7 pathway regulates proliferation and neurogenesis in neural precursors. Proc Natl Acad Sci USA. 2013 Aug 6;110(32):E3017-3026.
9. Pevny LH, Sockanathan S, Placzek M, Lovell-Badge R. A role for SOX1 in neural determination. Development. 1998 May;125(10):1967–78.

10. Mignone JL, Kukekov V, Chiang A-S, Steindler D, Enikolopov G. Neural stem and progenitor cells in nestin-GFP transgenic mice. J Comp Neurol. 2004 Feb 9;469(3):311–24.
11. Curto GG, Gard C, Ribes V. Structures and properties of PAX linked regulatory networks architecting and pacing the emergence of neuronal diversity. Semin Cell Dev Biol. 2015 Aug;44:75–86.
12. Dejosez M, Levine SS, Frampton GM, Whyte WA, Stratton SA, Barton MC, et al. Ronin/Hcf-1 binds to a hyperconserved enhancer element and regulates genes involved in the growth of embryonic stem cells. Genes Dev. 2010 Jul 15;24(14):1479–84.
13. Dejosez M, Krumenacker JS, Zitur LJ, Passeri M, Chu L-F, Songyang Z, et al. Ronin is essential for embryogenesis and the pluripotency of mouse embryonic stem cells. Cell. 2008 Jun 27;133(7):1162–74.
14. Jolly LA, Nguyen LS, Domingo D, Sun Y, Barry S, Hancarova M, et al. HCFC1 loss-of-function mutations disrupt neuronal and neural progenitor cells of the developing brain. Hum Mol Genet. 2015 Jun 15;24(12):3335–47.
15. Huang L, Jolly LA, Willis-Owen S, Gardner A, Kumar R, Douglas E, et al. A Noncoding, Regulatory Mutation Implicates HCFC1 in Nonsyndromic Intellectual Disability. Am J Hum Genet. 2012 Oct 5;91(4):694–702.
16. Quintana AM, Yu H-C, Brebner A, Pupavac M, Geiger EA, Watson A, et al. Mutations in THAP11 cause an inborn error of cobalamin metabolism and developmental abnormalities. Human Molecular Genetics. 2017 Aug;26(15):2838–2849.
17. Minocha S, Herr W. Cortical and Commissural Defects Upon HCF-1 Loss in Nkx2.1-Derived Embryonic Neurons and Glia [Internet]. Developmental Neurobiology. 2019 [cited 2019 Jul 19]. Available from: https://onlinelibrary.wiley.com/doi/abs/10.1002/dneu.22704
18. Michaud J, Praz V, Faresse NJ, Jnbaptiste CK, Tyagi S, Schütz F, et al. HCFC1 is a common component of active human CpG-island promoters and coincides with ZNF143, THAP11, YY1, and GABP transcription factor occupancy. Genome Res. 2013 Apr 25;
19. Yu H-C, Sloan JL, Scharer G, Brebner A, Quintana AM, Achilly NP, et al. An X-Linked Cobalamin Disorder Caused by Mutations in Transcriptional Coregulator HCFC1. Am J Hum Genet. 2013 Sep 5;93(3):506–14.
20. Quintana AM, Geiger EA, Achilly N, Rosenblatt DS, Maclean KN, Stabler SP, et al. Hcfc1b, a zebrafish ortholog of HCFC1, regulates craniofacial development by modulating mmachc expression. Dev Biol. 2014 Dec 1;396(1):94–106.
21. Minocha S, Sung T-L, Villeneuve D, Lammers F, Herr W. Compensatory embryonic response to allele-specific inactivation of the murine X-linked gene Hcfc1. Dev Biol. 2016 Apr 1;412(1):1–17.
22. Minocha S, Bessonnard S, Sung T-L, Moret C, Constam DB, Herr W. Epiblast-specific loss of HCF-1 leads to failure in anterior-posterior axis specification. Dev Biol. 2016 Oct 1;418(1):75–88.
23. An S, Park U-H, Moon S, Kang M, Youn H, Hwang J-T, et al. Asxl1 ablation in mouse embryonic stem cells impairs neural differentiation without affecting self-renewal. Biochem Biophys Res Commun. 2019 Jan 15;508(3):907–13.

24. Youn HS, Kim T-Y, Park U-H, Moon S-T, An S-J, Lee Y-K, et al. Asxl1 deficiency in embryonic fibroblasts leads to cellular senescence via impairment of the AKT-E2F pathway and Ezh2 inactivation. Sci Rep. 2017 Jul 12;7(1):5198.
25. Ablain J, Durand EM, Yang S, Zhou Y, Zon LI. A CRISPR/Cas9 vector system for tissue-specific gene disruption in zebrafish. Dev Cell. 2015 Mar 23;32(6):756–64.
26. Hwang WY, Fu Y, Reyon D, Maeder ML, Tsai SQ, Sander JD, et al. Efficient genome editing in zebrafish using a CRISPR-Cas system. Nat Biotechnol. 2013 Mar;31(3):227–9.
27. Hwang WY, Fu Y, Reyon D, Maeder ML, Tsai SQ, Sander JD, et al. Efficient genome editing in zebrafish using a CRISPR-Cas system. Nat Biotechnol. 2013 Mar;31(3):227–9.
28. Kwan KM, Fujimoto E, Grabher C, Mangum BD, Hardy ME, Campbell DS, et al. The Tol2kit: a multisite gateway-based construction kit for Tol2 transposon transgenesis constructs. Dev Dyn. 2007 Nov;236(11):3088–99.
29. Atlas of Zebrafish Development [Internet]. Elsevier; 2012 [cited 2019 Nov 25]. Available from: https://linkinghub.elsevier.com/retrieve/pii/C20090016171
30. Atlas of Early Zebrafish Brain Development [Internet]. Elsevier; 2016 [cited 2019 Nov 25]. Available from: https://linkinghub.elsevier.com/retrieve/pii/C20130006391
31. Thisse C, Thisse B. High-resolution in situ hybridization to whole-mount zebrafish embryos. Nat Protoc. 2008;3(1):59–69.
32. Thisse C, Thisse B. High-resolution in situ hybridization to whole-mount zebrafish embryos. Nat Protocols. 2008 Jan;3(1):59–69.
33. Bolger AM, Lohse M, Usadel B. Trimmomatic: a flexible trimmer for Illumina sequence data. Bioinformatics. 2014 Aug 1;30(15):2114–20.
34. Kim D, Pertea G, Trapnell C, Pimentel H, Kelley R, Salzberg SL. TopHat2: accurate alignment of transcriptomes in the presence of insertions, deletions and gene fusions. Genome Biol. 2013 Apr 25;14(4):R36.
35. Trapnell C, Roberts A, Goff L, Pertea G, Kim D, Kelley DR, et al. Differential gene and transcript expression analysis of RNA-seq experiments with TopHat and Cufflinks. Nat Protoc. 2012 Mar 1;7(3):562–78.
36. Bergsland M, Ramsköld D, Zaouter C, Klum S, Sandberg R, Muhr J. Sequentially acting Sox transcription factors in neural lineage development. Genes Dev. 2011 Dec 1;25(23):2453–64.
37. Ellis P, Fagan BM, Magness ST, Hutton S, Taranova O, Hayashi S, et al. SOX2, a persistent marker for multipotential neural stem cells derived from embryonic stem cells, the embryo or the adult. Dev Neurosci. 2004 Aug;26(2–4):148–65.
38. Hutton SR, Pevny LH. SOX2 expression levels distinguish between neural progenitor populations of the developing dorsal telencephalon. Developmental Biology. 2011 Apr 1;352(1):40–7.
39. Shen M-C, Ozacar AT, Osgood M, Boeras C, Pink J, Thomas J, et al. Heat-shock–mediated conditional regulation of hedgehog/gli signaling in zebrafish. Developmental Dynamics. 2013;242(5):539–49.

40. Pinto D, Delaby E, Merico D, Barbosa M, Merikangas A, Klei L, et al. Convergence of genes and cellular pathways dysregulated in autism spectrum disorders. American Journal of Human Genetics. 2014 May;94(5):677–694.
41. Gou Y, Guo J, Maulding K, Riley BB. sox2 and sox3 cooperate to regulate otic/epibranchial placode induction in zebrafish. Dev Biol. 2018 Mar 1;435(1):84–95.
42. Pan X, Sittaramane V, Gurung S, Chandrasekhar A. Structural and Temporal Requirements of Wnt/PCP Protein Vangl2 Function for Convergence and Extension Movements and Facial Branchiomotor Neuron Migration in Zebrafish. Mech Dev. 2014 Feb;131:1–14.
43. Wong T-T, Collodi P. Inducible Sterilization of Zebrafish by Disruption of Primordial Germ Cell Migration. PLoS One [Internet]. 2013 Jun 27 [cited 2019 Nov 25];8(6). Available from: https://www.ncbi.nlm.nih.gov/pmc/articles/PMC3694954/
44. Uni M, Kurokawa M. Role of ASXL1 mutation in impaired hematopoiesis and cellular senescence. Oncotarget. 2018 Dec 7;9(96):36828–9.
45. Hoischen A, van Bon BWM, Rodríguez-Santiago B, Gilissen C, Vissers LELM, de Vries P, et al. De novo nonsense mutations in ASXL1 cause Bohring-Opitz syndrome. Nat Genet. 2011 Aug;43(8):729–31.
46. Stainier DYR, Raz E, Lawson ND, Ekker SC, Burdine RD, Eisen JS, et al. Guidelines for morpholino use in zebrafish. PLOS Genetics. 2017 Oct 19;13(10):e1007000.
47. Kalueff AV, Stewart AM, Gerlai R. Zebrafish as an emerging model for studying complex brain disorders. Trends Pharmacol Sci. 2014 Feb;35(2):63–75.
48. Zebrafish Larvae as a Behavioral Model in Neuropharmacology [Internet]. [cited 2020 Jan 27]. Available from: https://www.ncbi.nlm.nih.gov/pmc/articles/PMC6465999/
49. Vinckevicius A, Parker JB, Chakravarti D. Genomic Determinants of THAP11/ZNF143/HCFC1 Complex Recruitment to Chromatin. Mol Cell Biol. 2015 Dec;35(24):4135–46.
50. Pupavac M, Watkins D, Petrella F, Fahiminiya S, Janer A, Cheung W, et al. Inborn Error of Cobalamin Metabolism Associated with the Intracellular Accumulation of Transcobalamin-Bound Cobalamin and Mutations in ZNF143, Which Codes for a Transcriptional Activator. Hum Mutat. 2016 Sep;37(9):976–82.
51. Mangone M, Myers MP, Herr W. Role of the HCF-1 basic region in sustaining cell proliferation. PLoS ONE. 2010;5(2):e9020.
52. Goto H, Motomura S, Wilson AC, Freiman RN, Nakabeppu Y, Fukushima K, et al. A single-point mutation in HCF causes temperature-sensitive cell-cycle arrest and disrupts VP16 function. Genes Dev. 1997 Mar 15;11(6):726–37.
53. Julien E, Herr W. Proteolytic processing is necessary to separate and ensure proper cell growth and cytokinesis functions of HCF-1. EMBO J. 2003 May 15;22(10):2360–9.
54. Carrillo-Carrasco N, Chandler RJ, Venditti CP. Combined methylmalonic acidemia and homocystinuria, cblC type. I. Clinical presentations, diagnosis and management. J Inherit Metab Dis. 2012 Jan;35(1):91–102.

55. X-Linked Cobalamin Disorder (HCFC1) Mimicking Nonketotic Hyperglycinemia With Increased Both Cerebrospinal Fluid Glycine and Methylmalonic Acid. - PubMed - NCBI [Internet]. [cited 2020 Jan 27]. Available from: https://www.ncbi.nlm.nih.gov/pubmed/28363510
56. Zhang P, Chen Z, Li R, Guo Y, Shi H, Bai J, et al. Loss of ASXL1 in the bone marrow niche dysregulates hematopoietic stem and progenitor cell fates. Cell Discov. 2018;4:4.
57. Yang H, Kurtenbach S, Guo Y, Lohse I, Durante MA, Li J, et al. Gain of function of ASXL1 truncating protein in the pathogenesis of myeloid malignancies. Blood. 2018 18;131(3):328–41.
58. Inoue D, Fujino T, Sheridan P, Zhang Y-Z, Nagase R, Horikawa S, et al. A novel ASXL1-OGT axis plays roles in H3K4 methylation and tumor suppression in myeloid malignancies. Leukemia. 2018;32(6):1327–37.
59. Reyes-Nava, Nayeli G., Hernandez, Jose A., Castro, Victoria L., Reyes, Joel F., Castellanos, Barbara S., Quintana, Anita M. Zebrafish: A Comprehensive Model to Understand the Mechanisms Underlying Neurodevelopmental Disorders. In: Costa, Andres., Villalba, Eugenio., editors. Horizons in Neuroscience Research. Nova Biomedical; 2018.
60. Afrikanova T, Serruys A-SK, Buenafe OEM, Clinckers R, Smolders I, de Witte PAM, et al. Validation of the zebrafish pentylenetetrazol seizure model: locomotor versus electrographic responses to antiepileptic drugs. PLoS ONE. 2013;8(1):e54166.
61. Ciura S, Lattante S, Le Ber I, Latouche M, Tostivint H, Brice A, et al. Loss of function of C9orf72 causes motor deficits in a zebrafish model of amyotrophic lateral sclerosis. Ann Neurol. 2013 Aug;74(2):180–7.
62. Liu Y, Carmer R, Zhang G, Venkatraman P, Brown SA, Pang C-P, et al. Statistical Analysis of Zebrafish Locomotor Response. PLoS ONE. 2015;10(10):e0139521.
63. Li F, Lin J, Liu X, Li W, Ding Y, Zhang Y, et al. Characterization of the locomotor activities of zebrafish larvae under the influence of various neuroactive drugs. Ann Transl Med. 2018 May;6(10):173.
64. Kalueff AV, Gebhardt M, Stewart AM, Cachat JM, Brimmer M, Chawla JS, et al. Towards a Comprehensive Catalog of Zebrafish Behavior 1.0 and Beyond. Zebrafish. 2013 Mar;10(1):70–86.
65. Lattante S, de Calbiac H, Le Ber I, Brice A, Ciura S, Kabashi E. Sqstm1 knock-down causes a locomotor phenotype ameliorated by rapamycin in a zebrafish model of ALS/FTLD. Hum Mol Genet. 2015 Mar 15;24(6):1682–90.
66. Bonnin E, Cabochette P, Filosa A, Jühlen R, Komatsuzaki S, Hezwani M, et al. Biallelic mutations in nucleoporin NUP88 cause lethal fetal akinesia deformation sequence. PLoS Genet. 2018;14(12):e1007845.

Tables

Table 1: RNA-Sequencing reveals 36 upregulated and downregulated genes.

Gene Name	Gene ID	Fold Change
si:dkey-222f8.6	XLOC_021011	14.4930988
asxl1	XLOC_016905	3.85582801
ccl44	XLOC_003025	3.76589623
zgc:112970	XLOC_030718	3.45845584
si:dkey-15j16.6	XLOC_014036	2.66543586
mucms1	XLOC_001109	2.59007221
CR388052.1	XLOC_023401	2.44522307
si:dkey-15j16.3	XLOC_014035	2.39033346
CABZ01017723.1	XLOC_031170	2.23752184
cart3	XLOC_028234	2.10261498
SLC22A3	XLOC_009181	1.97809228
camk1gb	XLOC_017012	1.91222151
vtg1,vtg4,vtg5,vtg6,vtg7	XLOC_016435	1.91072755
si:dkey-208m12.2	XLOC_016485	1.88711718
usp48	XLOC_003342	1.88552791
si:dkey-85k7.7	XLOC_027050	1.86192429
znf319	XLOC_018986	1.75290426
si:dkey-14o1.18	XLOC_029699	1.73919114
cry-dash	XLOC_018109	1.68379868
si:ch73-60p2.1	XLOC_016151	1.67438066
hbbe3	XLOC_004139	1.64033724
c3b.1,c3b.2	XLOC_016458	1.53598227
hcfc1a	XLOC_003246	0.68365388
fut9d	XLOC_028523	0.6648173
si:ch211-183d21.1	XLOC_017905	0.58211004
exosc3	XLOC_031084	0.55764572
si:dkey-147f3.4	XLOC_016723	0.55397064
cox6b1	XLOC_018338	0.54151104
BX530067.1	XLOC_011301	0.53422498
si:dkey-57c15.9	XLOC_016192	0.50905352
si:dkey-9l20.3	XLOC_016618	0.47144985
slc23a3	XLOC_030187	0.34691461
wu:fi09b08	XLOC_031057	0.34631257
hsp70l	XLOC_028453	0.27760694
si:dkey-51a16.10	XLOC_004659	0

Illumina Sequencing was performed on triplicates of whole brain homogenates from 2dpf *hcfc1a*+/^{co60} allele zebrafish larvae (N=12). Analysis revealed 23 upregulated (Green cells) and 14 downregulated (Red Cells) genes with statistical significance of 2.5 x 10^{-5} or greater.

Figures

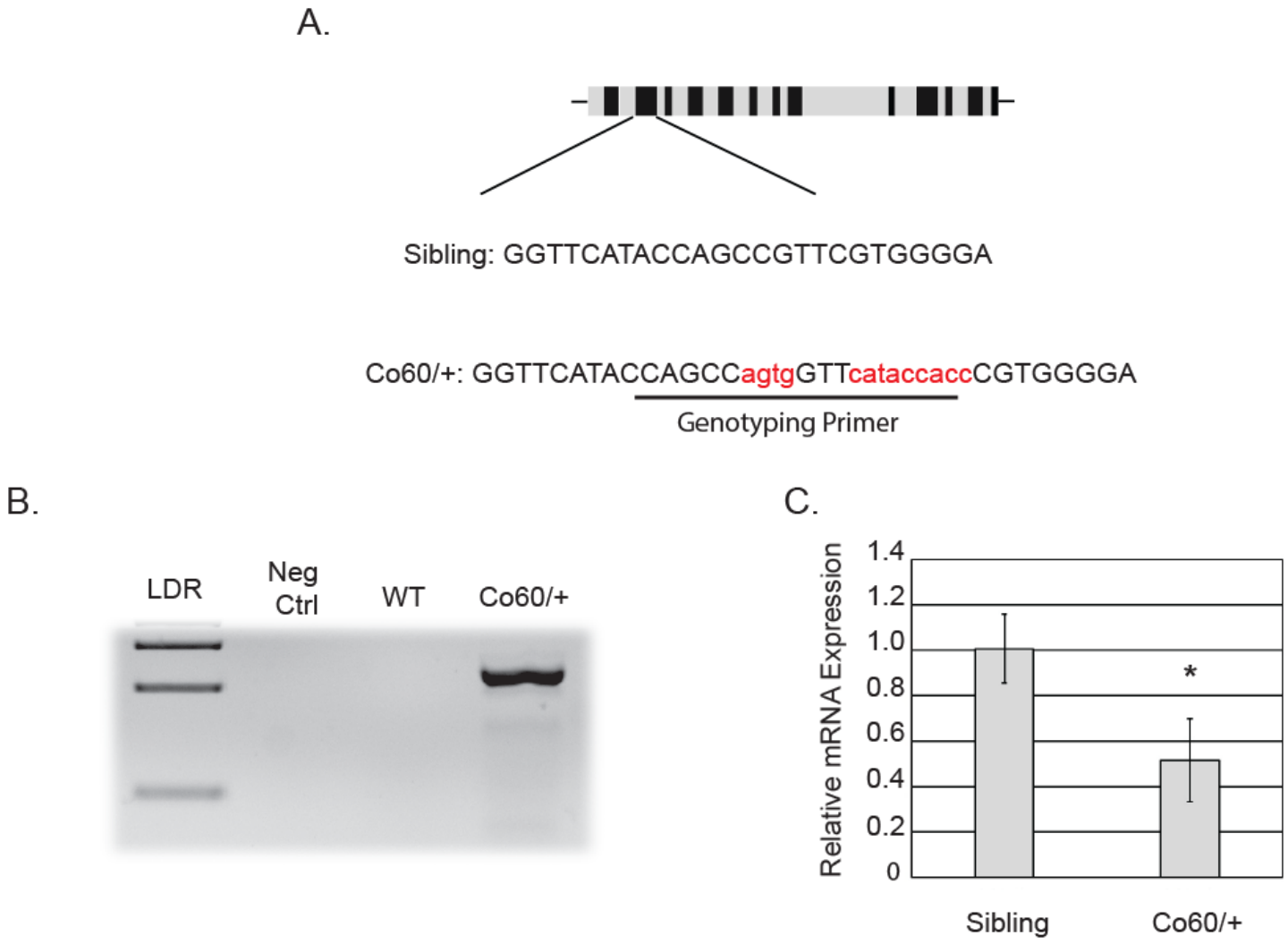

Figure 1

Haploinsufficiency of the hcfc1aco60/+ allele (Co60/+). A. Schematic of the exon structure of the hcfc1a gene. The gRNA produced targets the sequence shown within exon 4 (Sibling). The Co60 allele results in an insertion of 13 nucleotides (Red). B. Primers were designed to specifically amplify the Co60 allele. The specific primer is underlined and bolded in the sequence presented in (A). Positive amplification is indicative of heterozygous carriers (Co60/+) with no amplification of the wildtype allele (WT). C. Quantitative real time PCR analyzing the relative expression of hcfc1a in wildtype siblings (Sibling) and the hcfc1aco60/+ allele (Co60/+) at 2 days post fertilization. N=16 larvae per group with 3 biological replicates. *p<0.05

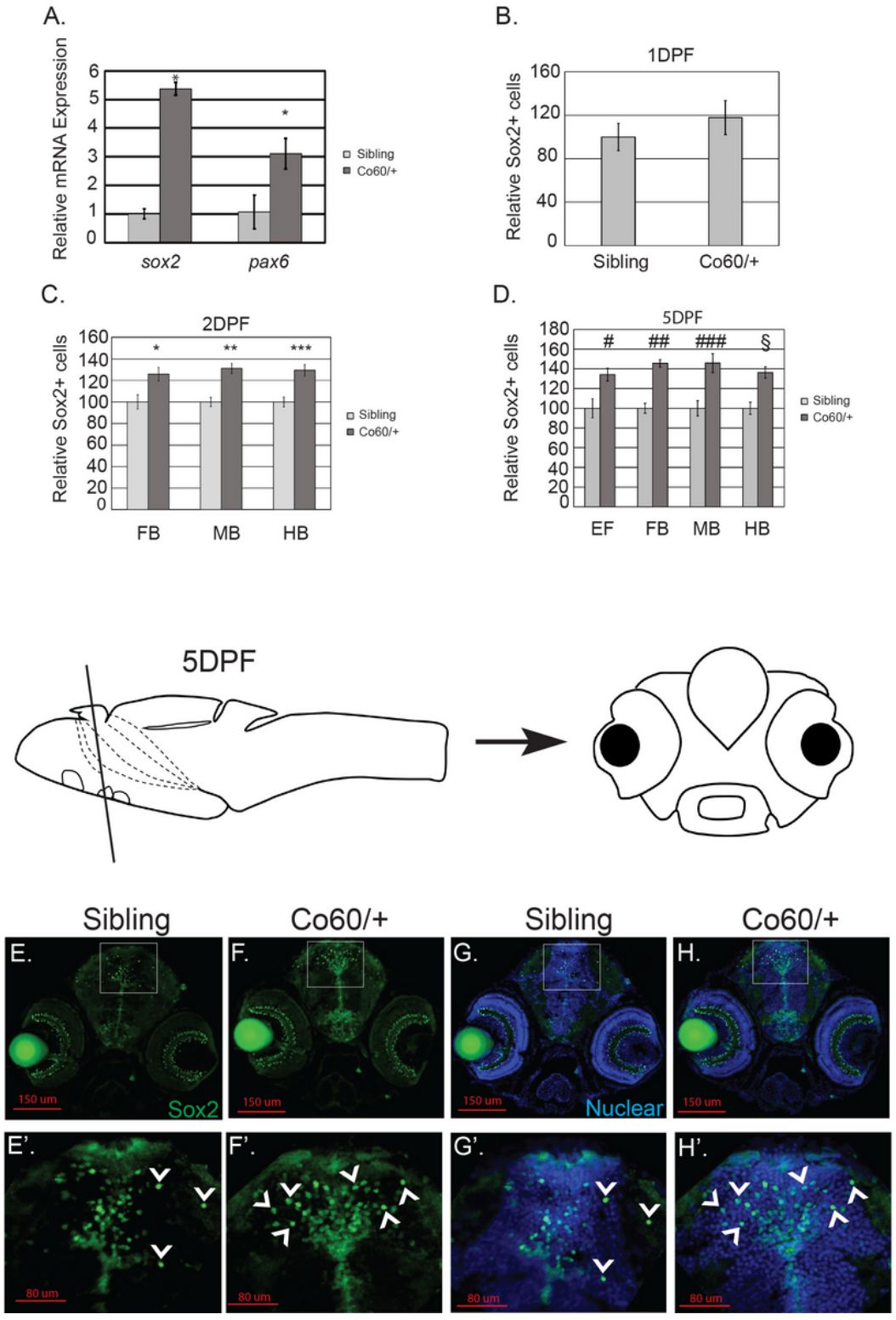

Figure 2

The hcfc1aco60/+ allele increases the number of Sox2+ cells in the developing brain. A. Quantitative real time PCR analyzing the relative expression of sox2 and pax6 in wildtype siblings (Sibling) and the hcfc1aco60/+ allele (Co60/+). N=7 larvae per group *p<0.05. B-D. Quantification of the number of Sox2+ cells at 1 day post fertilization (DPF) (B), 2 DPF (C), and 5 DPF (D) in the early forebrain (EF), forebrain (FB), midbrain (MB), and hindbrain (HB). *p=0.006828, **p= 1.13873E-05, ***p= 0.000107, #p= 0.010168,

##p= 4.55E-06, ###p= 1.97E-07, and §p= 0.005476. In B total number of animals is Sibling (N=6) and hcfc1aco60/+ (N=6), C total animals is Sibling (N=7) and hcfc1aco60/+ (N=7), and D total animals is Sibling (N=4) and hcfc1aco60/+ (N=4). All error bars represent standard error of the mean. E-H&E'-H'. Representative images of brain sections from larvae at 5 DPF stained with Sox2 antibodies (green) and Hoescht DNA content dye. Whole brain (20X) and the ventricular zone (63X) are shown. A schematic of the zebrafish 5 day brain is shown above representative images with a line to indicate the section shown below.

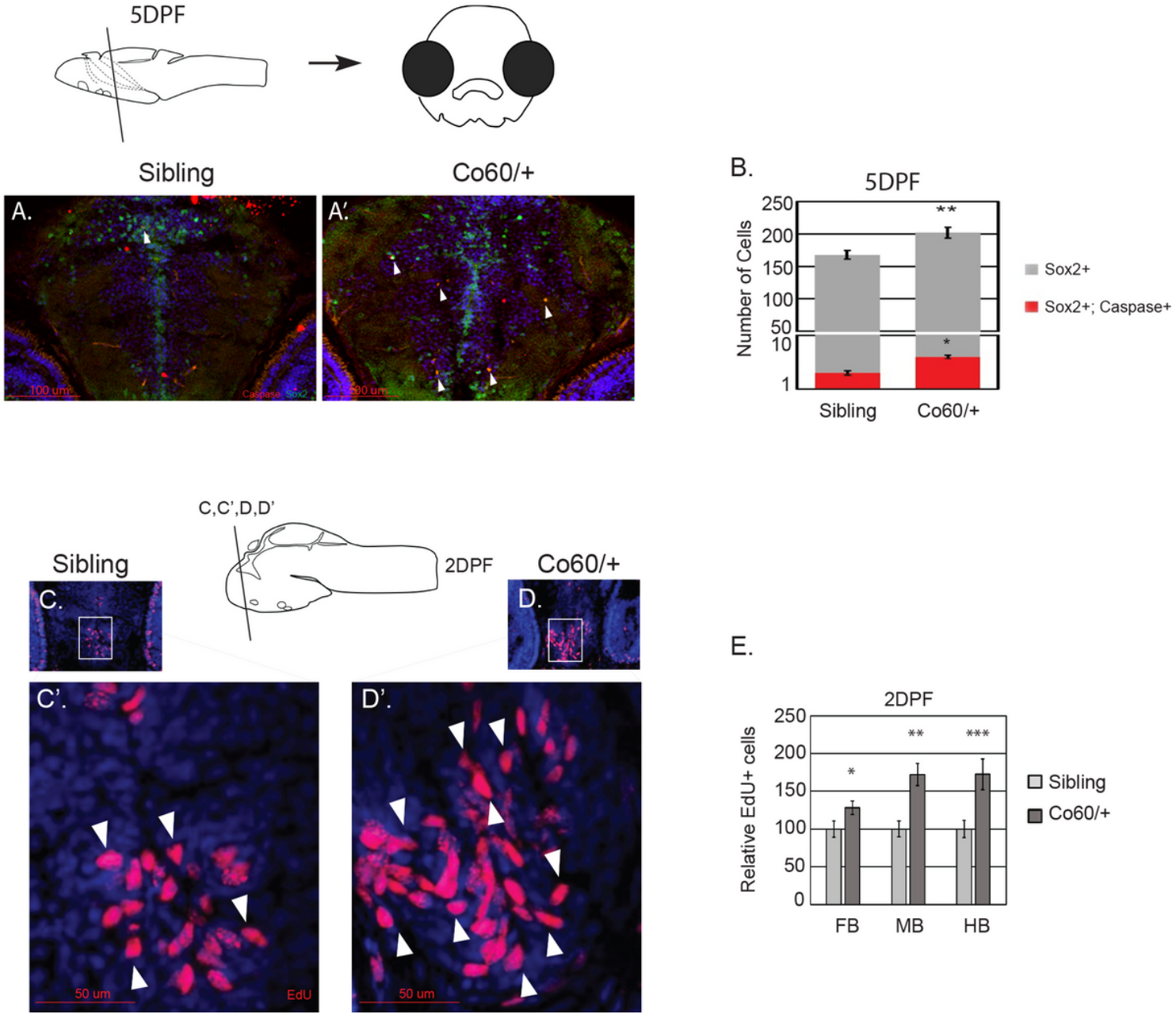

Figure 3

The hcfc1aco60/+ allele is associated with increased cell proliferation and minimal cell death. A-A'. Apoptosis of Sox2+ neural precursor cells was assessed using anti-caspase 3 and anti-Sox2 antibodies at 5 days post fertilization (DPF). Representative images are depicted from sibling wildtype (Sibling) or

the hcfc1aco60/+ allele (Co60/+). Arrows indicate Sox2+ caspase+ neural precursors. B. The total number of Sox2+ Caspase+ cells was quantified in wildtype siblings and the Co60/+ allele. Independently, the total number of Sox2+ was also quantified and the graph depicts the total number of Caspase positive NPCs (red bars; * P= 1.47822E-16) present within the entire Sox2+ population (gray bars; **P<0.05). Due to the small number of total Sox2+ Caspase+ cells present, the data is depicted as total numbers of cells in the entire brain. N=3/group. C-D&C'-D'. Representative images of larvae (Sibling or Co60/+) pulsed with ethynyl-deoxyuridine (EdU) to monitor cell proliferation at 2DPF. C&D are 20X magnifications and C'&D' represent region in the inset at 63X magnification. E. Quantification of the total number of EdU positive cells in forebrain (FB), midbrain (MB), and hindbrain (HB) of siblings and hcfc1aco60/+ larvae at 2 DPF. *p= 0.060553, **p= 0.00108, ***p= 0.006642, N=9 per group. All error bars represent standard error of the mean.

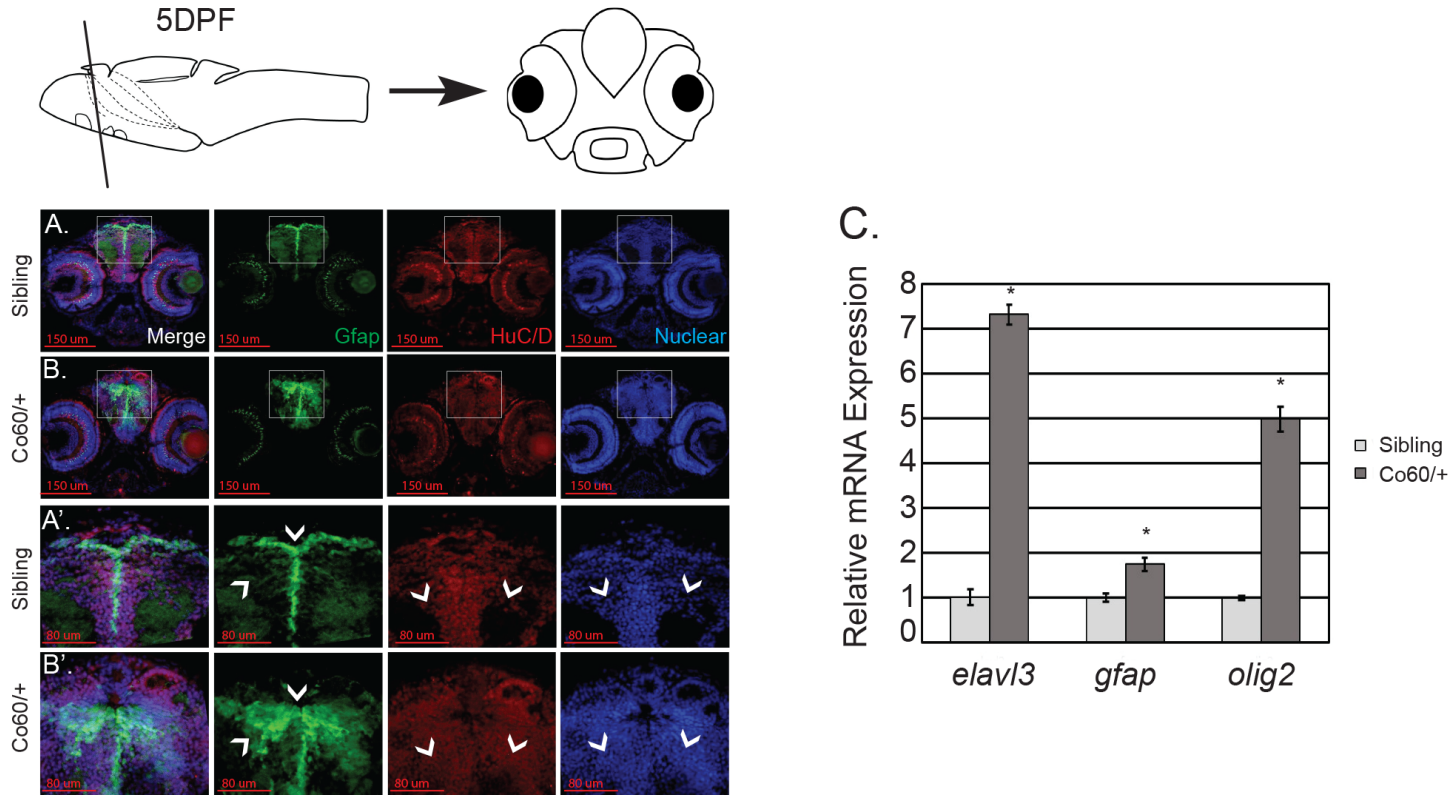

Figure 4

The hcfc1aco60/+ allele increases the expression of differentiation markers. A, A', B,&B'. Representative images of brain sections from Tg(gfap:EGFP) larvae harboring the hcfc1aco60/+ allele (Co60/+) at 5 days post fertilization (DPF) stained with Elavl3 (HuC/D) antibodies and Hoescht DNA content dye. 20X representatives of the entire brain (A-B) and 63X sub-regions (A'-B') are shown. Wildtype siblings (N=6) and hcfc1aco60/+ larvae (N=6). Arrowheads indicate regions of increased expression/localization of protein. Arrowheads of Hoescht (Nuclear) images demonstrate regions with cell bodies. Top schematic demonstrates a 5 DPF larval brain with a line to demonstrate the region depicted below. C. Quantitative real time PCR analysis of the expression of elavl3, gfap, and olig2 in siblings and hcfc1aco60/+ larvae (N=8/group). Error bars represent standard error of the mean. * P<0.05.

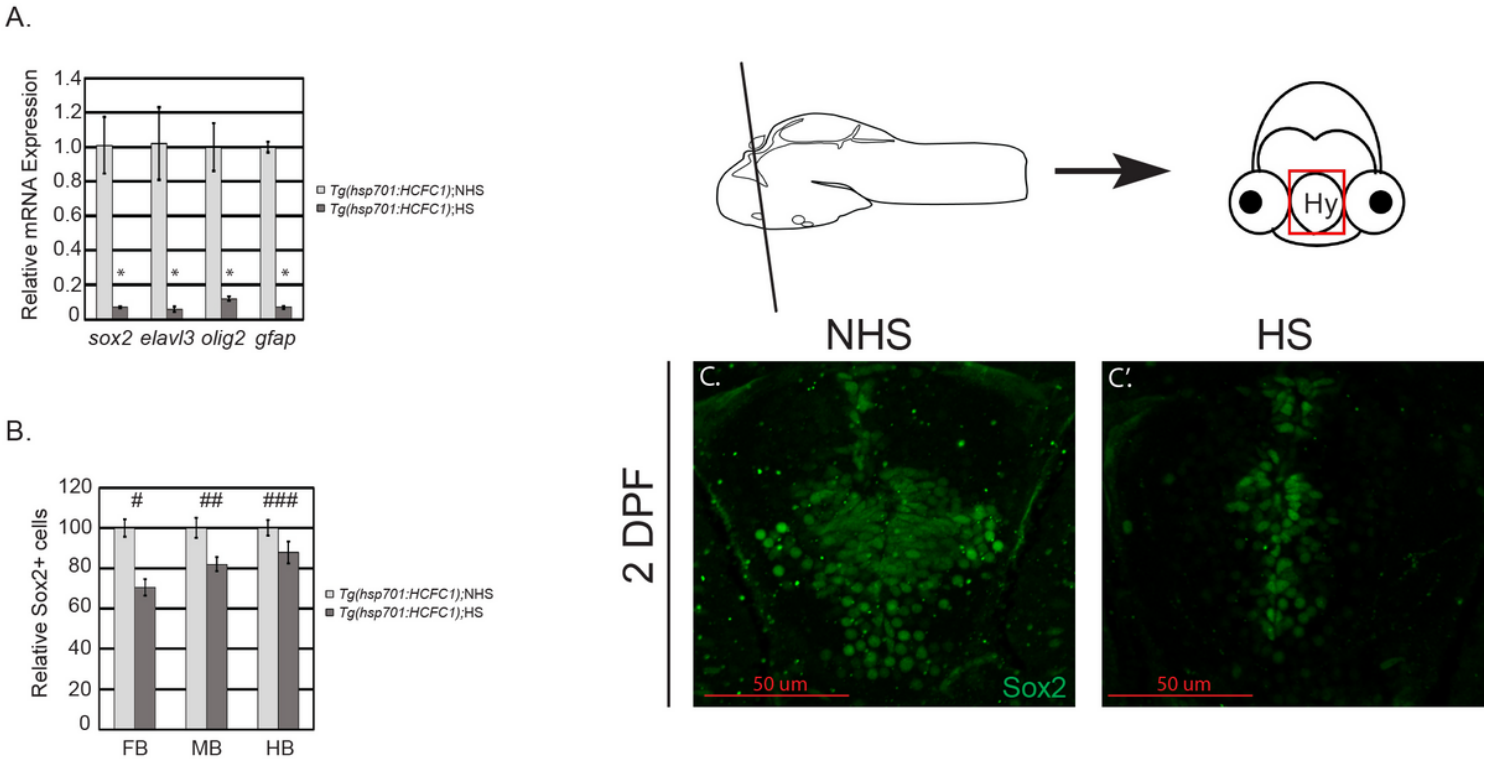

Figure 5

Over expression of HCFC1 decreases NPC number and differentiation. A. Tg(hsp701: HCFC1) were heat shocked according to the Methods section and total RNA was isolated from control (No heat shock (NHS)) and heat shock (HS). Quantitative PCR was performed to test the expression of sox2, elavl3, olig2, and gfap. Error bars represent standard error of the mean. N=28/group. *P<0.05. B. The total number of Sox2 cells was quantified across forebrain (#P= 4.88568E-05), midbrain (##P= 0.004359), and hindbrain (###P=0.077). Error bars represent standard error of the mean. N=5/group. C&C'. Representative images of 2 days post fertilization (DPF) Tg(hsp701:HCFC1) larvae (NHS or HS) stained with anti-Sox2 antibodies. Schematic demonstrates 2 DPF larval brain section with graphical inset of hypothalamus region (Hy) to specify region shown.

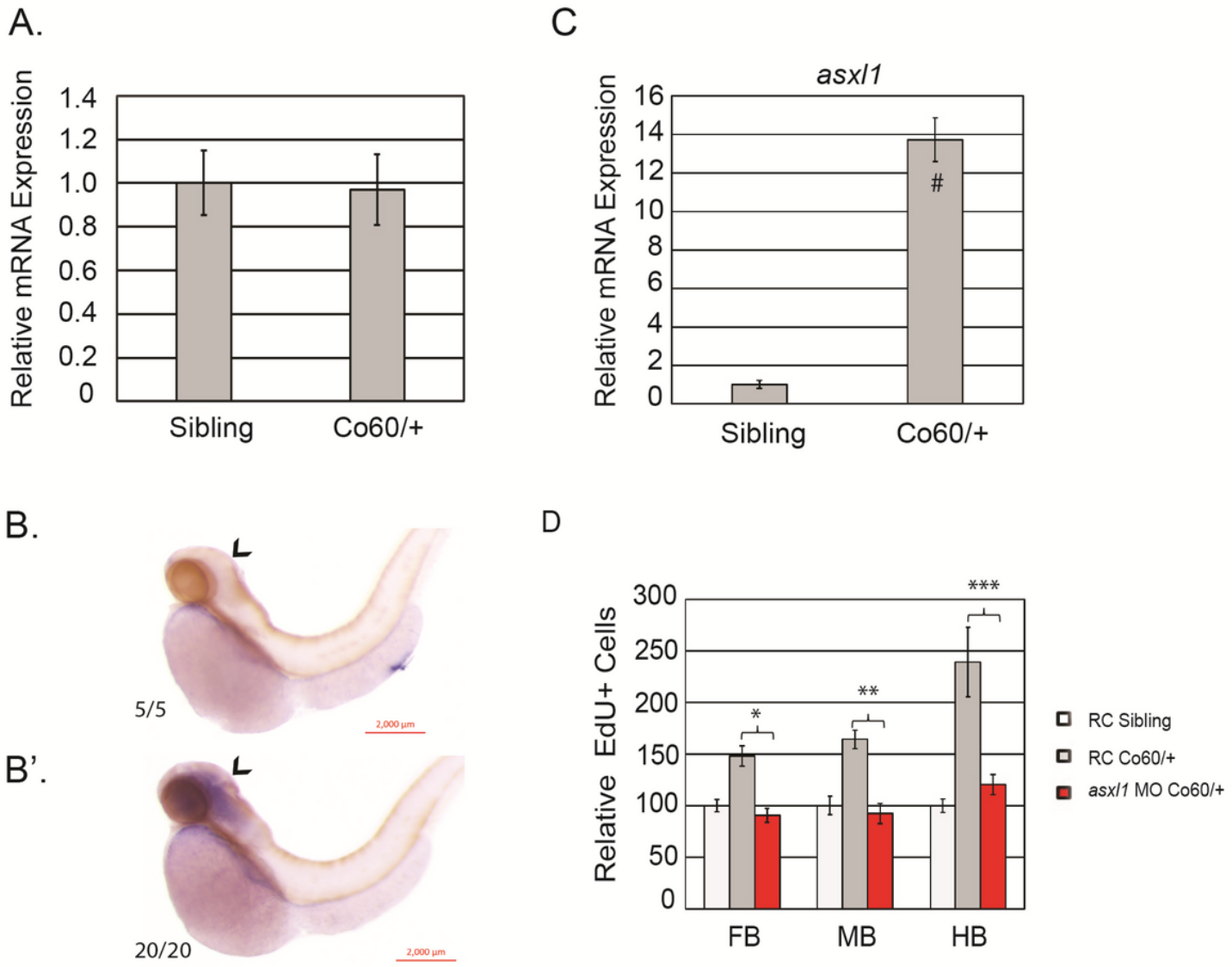

Figure 6

The hcfc1aco60/+ allele regulates brain development and asxl1 expression. A. Quantitative real time PCR (QPCR) analyzing the relative expression of mmachc in wildtype siblings (Sibling) and hcfc1aco60/+ larvae (Co60/+). N=16 larvae per group with 3 biological replicates. (B&B') Whole mount in situ hybridization (ISH) was performed at 2 days post fertilization (DPF) using a riboprobe targeting asxl1 mRNA. ISH was performed with sense control (B) and anti-sense specific probe (B'). Purple demonstrates positive staining in the developing brain. N= 21. C. QPCR analyzing the relative expression of asxl1 in wildtype siblings (Sibling) and the hcfc1aco60/+ allele. N=16 larvae per group with 3 biological replicates. # $p<0.05$. D. hcfc1aco60/+ larvae (Co60/+) and their wildtype siblings (Sibling) were injected with translation inhibiting morpholinos targeting asxl1 (asxl1 MO) or random control (RC) morpholinos. At 2 DPF larvae were pulsed and stained for EdU incorporation and the number of EdU positive cells was counted per brain section and the total number of cells in the forebrain (FB), midbrain (MB), and hindbrain (HB) was calculated. *$p=0.000127$, **$p=0.000407$, ***$p=0.00712$. N=6/group.

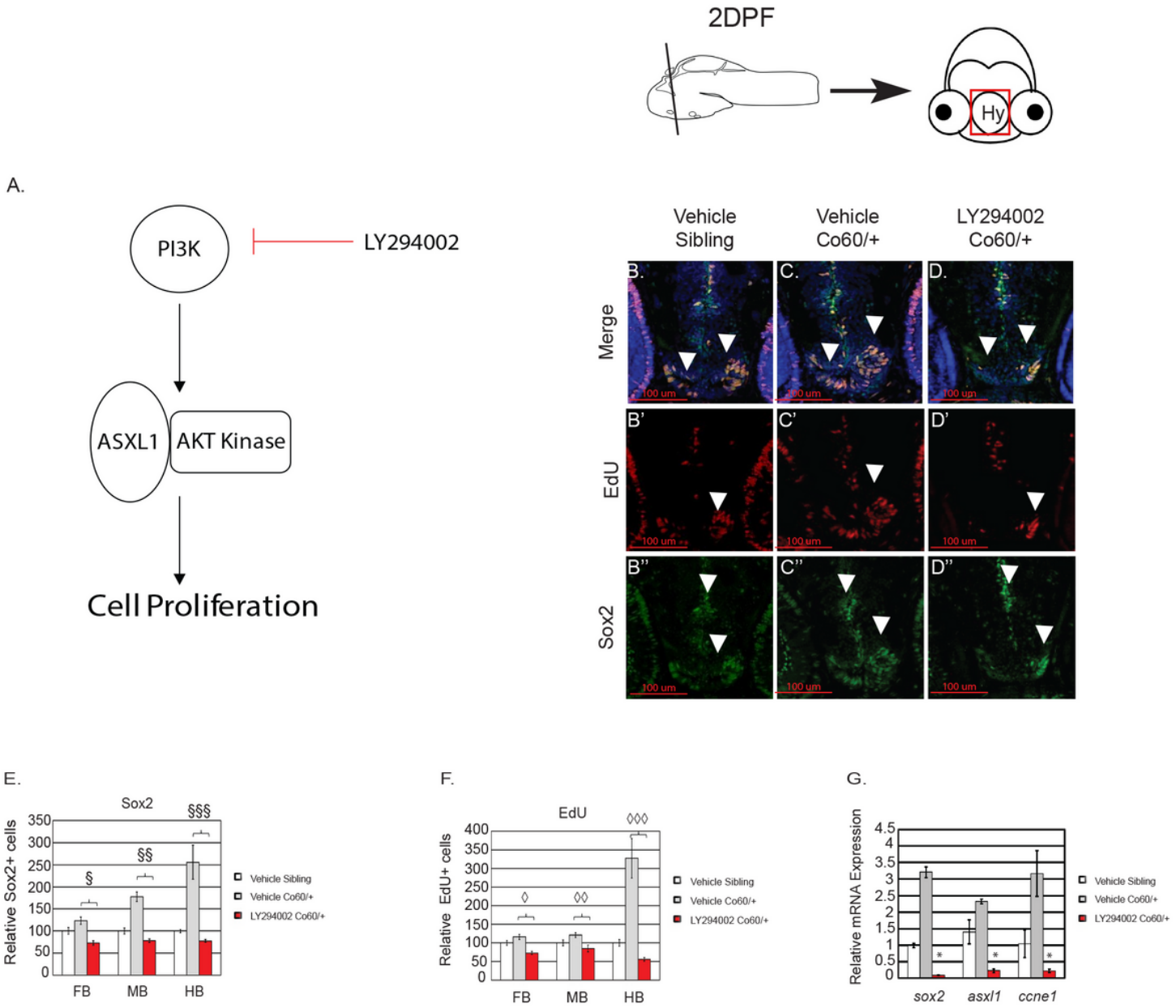

Figure 7

Inhibition of Asxl1 activity restores the NPC deficits in the hcfc1aco60/+ allele. A. Summary diagram of the known function of Asxl1 in promoting cell proliferation. Diagram adapted from data published by Youn and colleagues (24). Treatment with PI3K inhibitor LY294002 is known to abolish the function of Asxl1 in mice. B-B", C-C", D-D". Representative 20X images of Sibling wildtype (B-B"), hcfc1aco60/+ larvae (Co60/+) (C-C"), or Co60/+ larvae treated with 12uM LY294002 (D-D") at 2 days post fertilization (DPF). Schematic of 2 DPF brain with a line marking the region shown is presented above representative images. E&F. Quantification of the number of Sox2+(E) or EdU (F) positive cells in vehicle treated and larvae treated with LY294002 at 2 DFP. N= 4 Vehicle Sibling, 6 Vehicle hcfc1aco60/+ larvae, and 4 LY294002 hcfc1aco60/+ larvae. §p=0.000168, §§p=2.08852E-09, §§§p=0.000153. ◊p=7.22142E-07, ◊◊p=0.000997, ◊◊◊p=0.00014. All error bars represent standard error of the mean. G. hcfc1aco60/+ larvae and their wildtype siblings (Sibling) were treated at 24 hour intervals with 12uM LY294002 until 5

DPF and then total RNA was isolated from brain homogenates. Quantitative real time PCR was performed to test the expression of sox2, asxl1, and cyclin E (ccne1). N=10/group. Error bars represent standard error of the mean. *P<0.05

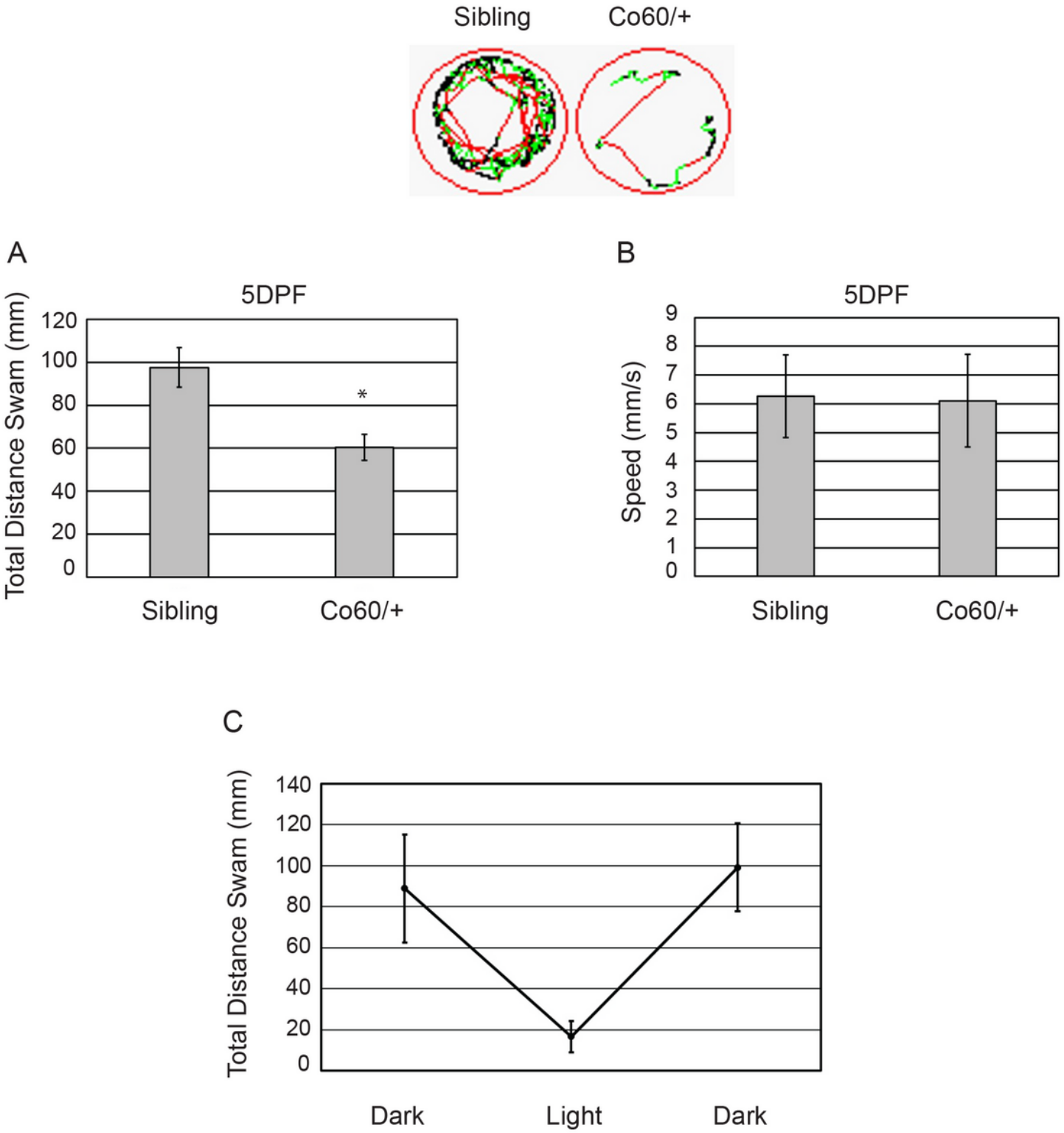

Figure 8

The hcfc1aco60/+ is associated with hypomotility. Total distance (A) and average speed (B) of wildtype (Sibling) and heterozygous carriers of the hcfc1aco60/+ (Co60/+) allele were tracked at 5 days post

fertilization (DPF) using ZebraBox technology. Distance and speed were monitored after light stimulus for a 5 minute duration. Top panel shows representative tracking patterns from Sibling wildtype and heterozygous carriers of the Co60/+ allele. *p<0.001. N=52 Sibling wildtype and 56 Co60/+ individual larvae. C. 5 DPF larvae were monitored for total distance swam in alternating dark-light conditions.

Supplementary Files

This is a list of supplementary files associated with this preprint. Click to download.

- SupplementalFigure1.docx